Supporting Information

Cold-resistant, highly stretchable ionic conductive hydrogel for intelligent motion recognition in winter sports

Tongda Lei [a], Jiajun Pan [a], Ning Wang [a], Zhaopeng Xia [a, *], Qingsong Zhang [b, *], Jie Fan [a, *], Lei Tao [c], Wan Shou [d], Yu Gao [b]

[a] *School of Textile Science and Engineering, Tiangong University, Tianjin 300387, China*

[b] *School of Material Science and Engineering, Tiangong University, Tianjin 300387, China*

[c] *The Key Laboratory of Bioorganic Phosphorus Chemistry and Chemical Biology (Ministry of Education), Department of Chemistry, Tsinghua University, Beijing 100084, PR. China*

[d] *Department of Mechanical Engineering, University of Arkansas, Fayetteville, AR 72701, USA*

Experimental section

Materials

Poly (vinyl alcohol) (PVA, degree of alcoholysis: 98–99% (mol/mol), and polymerization degree 1799), sodium carboxymethyl cellulose (CMC, 300 - 800 mPa·s) , acrylamide (AAm, 99%) and ammonium persulfate (APS, ⩾98%) were purchased from Aladdin Chemical Reagent Co., Ltd. (Shanghai, China). 1-vinyl-3-butylimidazolium bromide (VBIMBr, 99%) and *N, N, N', N'*-tetramethyl ethylenediamine (TEMED, 99%) were obained from Macklin Biochemical Technology Co., Ltd. (Shanghai, China). N, N'-Methylenebisacrylamide (MBAA, 97 %) were ordered from Shanghai Bide Pharmaceutical Technology Co., Ltd. (Shanghai, China). All chemicals reagents used in this study were analytical grade and used as received without further purification. Deionized water (18.25 MΩ·cm) was used for all the experiments. *Escherichia coli* (*E. coli*, ATCC 25922) and *Staphylococcus aureus* (*S. aureus*, ATCC 6538) were obtained from Shanghai Luwei Technology Co., Ltd., China.

Preparation of PCPAV ionic conductive hydrogels

Ionic conductive hydrogels were synthesized via a simple two-step approach of free radical polymerization and freeze-thaw cycling. First, PVA (0.8 g) was dissolved in distilled water (9.2 g) under magnetic stirring at 90 °C for 2 h to obtain an 8wt% PVA aqueous solution. The CMC powder was subsequently added to the PVA solution

and stirred until the formation of a transparent solution. Then, functional monomer AAm (2.0 g) and VBIMBr (2.0 g), crosslinking agent MBAA (0.1wt% of AAm and VBIMBr) were added to PVA/CMC solution in sequence. After thoroughly stirred at 25 °C, the initiator APS (1wt% of AAm and VBIMBr) and 30 μL TEMED (10% aqueous solutions) were added to the reaction system under continuing stirring. 10 min later, the resultant mixed solution was bubbled with nitrogen to remove oxygen. The well-mixed pre-gel solution was then poured into a mold and polymerized at 50 °C for 5 h. Finally, the glass molds were frozen in a refrigerator at -20 °C for 6 h and then thawed at 25 °C for 2 h. The process was repeated thrice to obtain PVA/CMC/P(AAm-*co*-VBIMBr) (PCPAV) ionic conductive hydrogels with the desired shape. The detailed feed ratios of PCPAV ionic conductive hydrogels were shown in Table S4, and named as PC_xPAV_y hydrogels, in which x and y meant the weight ratio (g) of CMC and VBIMBr in the PVA solution, respectively. Generally, x is 0-1.25%, and y is 0-30%. For example, PC_1PAV_{20} hydrogel indicates the weight ratio (g) of CMC and VBIMBr relatively to the PVA solution was 1% and 20%, respectively.

Characterization

Morphology and elemental mapping

The internal morphology and elemental mapping of the PCPAV conductive hydrogels were observed and analyzed using a field emission scanning electron microscope (FESEM, Hitachi Regulus 8100, Japan) and attached energy dispersive X-ray spectroscopy (EDS). To observe intact internal structure, the hydrogel samples were

firstly embrittled in liquid nitrogen, and then freeze-dried using a lyophilizer for 48 hours. All lyophilized hydrogel samples were sprayed with a thin gold layer using a sputter coater (Hitachi e-1030).

Fourier transform infrared spectroscopy (FTIR)

The chemical structure of the PCPAV conductive hydrogels was investigated using a FTIR spectrometer (Nicolet iS 20, Thermo Fisher Scientific, USA) in the wave number range of 400-4000 cm^{-1} with a resolution of 4 cm^{-1}. Before test, the hydrogel samples were freeze-dried in the lyophilizer for 48 hours.

X-ray diffraction (XRD) measurement

Crystallinity of the PCPAV conductive hydrogel samples was measured with an X-ray diffractometer (Rigaku Smartlab SE, Japan) from 5° to 90° (2θ) at a scanning speed of 5°/min.

X-ray photoelectron spectroscopy (XPS)

Elemental composition of lyophilized PC_1PAV_0 and PC_1PAV_{20} samples were measured using an X-ray photoelectron spectrometer (Thermo Fisher ESCALAB 250Xi, USA).

UV-visible transmittance test

The transmittance of PCPAV hydrogel samples with 2 mm thickness was recorded using an UV-Vis spectrophotometer (UV-2600, Japan) at a scanning rate of 100 nm/min

in the wavelength range of 200 to 800 nm. Before analysis, all samples were cut into rectangles of 30 mm in length and 10 mm in width.

Mechanical properties of hydrogels

Tensile and compression tests of the PCPAV conductive hydrogels were performed on an universal testing machine (HY-0580, China) with a 1 kN load cell. For the tensile tests, the size of the hydrogel samples was 50 mm in length, 5 mm in width and 2 mm in thickness with a clamping distance of 10 mm. All the samples were tested with a deformation rate of 10 mm/min at 25 °C. The samples for compression fatigue test were 12 mm in height and 15 mm in diameter. The tests were performed at 80% of the maximum strain with a fixed speed of 1 mm/min. The elastic modulus, toughness and dissipated energy were calculated from the stress-strain curves. The elastic modulus (E) was the slope of the initial linear region of the stress-strain curves. The toughness (T) was calculated by the integral area under the stress-strain curve, as shown in equation (1):

$$T = \int_{\varepsilon_0}^{\varepsilon_f} \sigma \, d\varepsilon \tag{1}$$

where ε_0 and ε_f denote the strains at initial tensile and fracture, respectively, and σ corresponds to the stress.

The dissipated energy (ΔT) was defined as the integral area of the cyclic loading-unloading curves, which is calculated as follows equation (2):

$$\Delta T = \int_{\text{loading}} \sigma \, d\varepsilon - \int_{\text{unloading}} \sigma \, d\varepsilon \tag{2}$$

All the mechanical tests were carried out 5 times and the average data were reported.

Anti-freezing and moisturizing behavior tests

The freezing resistance of the PCPAV hydrogel samples (5-10 mg) was analyzed using a differential scanning calorimeter (Mettler DSC 3, Switzerland). Before test, the test system was cooled from 20 °C to -70 °C under flowing nitrogen atmosphere (50 mL/min). After holding the temperature at -70 °C for 5 min, the samples were heated up to 25 °C at a heating rate of 5 °C/min.

The total water content (W_c) of the hydrogel could be calculated by equation (3):

$$W_c = \frac{m_h - m_d}{m_h} \times 100\% \quad (3)$$

where m_d is the weight of the dried hydrogel samples and m_h is the total mass of the hydrogel.

The freezing water content (W_f) is calculated according to equation (4):

$$W_f = \frac{\Delta H}{\Delta H_0} \times 100\% \quad (4)$$

where ΔH (units of J/g) is the melting enthalpy of the hydrogel, which could be obtained by integrating the endothermic peak in the DSC curve, and ΔH_0 (J/g) is the specific fusion enthalpy of pure water (334 J/g).

Therefore, the percentage of non-freezing water (W_{nf}) could be calculated as equation (5):

$$W_{nf} = W_c - W_f \quad (5)$$

Moisture retention of the PC_1PAV_0 and PC_1PAV_{20} hydrogels were evaluated by placing the hydrogels in an environment with a temperature of 25 °C and a relative humidity of approximately 50% for 7 days. The weight of the hydrogels was recorded every day and the moisture retention (W_r) was calculated by using the following equation (6):

$$W_r = W_t - W_0 \tag{6}$$

where W_t and W_0 correspond to the practical and dry weight of hydrogels, respectively.

Self-healing test of hydrogels

The PC_1PAV_{20} hydrogels were cut into several pieces, and then the newly cut surfaces were placed together at 25 °C without any external irritation. The self-healing properties of the hydrogels were evaluated by observing the change in the brightness of a light-emitting diode (LED) connected with the broken PC_1PAV_{20} hydrogels and a power supply. The breaking tensile strength of the self-healed hydrogel was determined by using the same universal testing machine mentioned above at a tensile speed of 10 mm/min, and the self-healing efficiency (HE, %) was used to quantitatively evaluate the self-healing capability of the hydrogels after different times of healing. HE is defined by the ratio of breaking tensile strength before and after hydrogel self-healing, which is calculated by the following equation (7):

$$HE = \frac{S_h}{S_o} \times 100\% \tag{7}$$

where S_h represented the breaking tensile strain of the hydrogel after self-healing and S_o represented the breaking tensile strain of the original hydrogel.

Antimicrobial tests

The antibacterial activity of PCPAV hydrogels were evaluated by *Escherichia coli* (*E. coli*, Gram-negative) and *Staphylococcus aureus* (*S. aureus*, Gram-positive). Before testing, all hydrogel samples were irradiated with UV light in an ultra-clean bench for more than 30 minutes. First, 20 mL of nutritional agar was poured into a disposable plastic culture dish and left to solidify. *E. coli* and *S. aureus* were incubated in peptone liquid medium at 37 °C for 24 h. After that, the bacterial concentration was adjusted to 1×10^6 CFU/mL. 1000 μL bacterial suspensions were inoculated into 100 mL sterilized peptone liquid medium, and then the sterilized PCPAV hydrogels were put into the above liquid medium and incubated in a shaker with 130 rpm at 37 °C for 24 hours. After that, the obtained bacterial suspension was diluted to 10^{-6} times of its original concentration, and 100 μL diluted bacterial suspension was pipetted onto nutritional agar plate medium with a pipette gun and spread evenly on the surface of the medium using a triangular applicator until solidified. After culturing at 37 °C for 24 hours, photographs were recorded using a digital camera and the colony forming unit (CFU) was counted. Each group of experiments was repeated three times and the average value was taken. The bacterial suspension without hydrogel was used as a blank control group. The inhibition rate was calculated using the following formula (8):

$$\text{Bactericidal ratio}\,(\%) = \frac{C_c - C_s}{C_c} \times 100\% \tag{8}$$

where C_c and C_s are the number of colonies in the control and hydrogel sample groups, respectively.

Electrical measurements

The resistance of rectangular hydrogel samples with a length of 15 mm, a width of 5 mm and a thickness of 2 mm was tested using a Keithley 2450 digital source meter (2450, Tektronix), and the ionic conductivity of the PCPAV conductive hydrogels was calculated using the following equation (9):

$$\sigma = \frac{L}{S} \times \frac{1}{R} \tag{9}$$

where σ, L, S and R represent the conductivity, length, cross-sectional area and resistance of the hydrogels, respectively. All tests were repeated at least three times at 25 °C.

Sensing properties of the PCPAV-based hydrogel strain sensors

The PCPAV hydrogel can be used as a wearable strain sensor by monitoring its resistance variations. The performance of the hydrogel sensors was evaluated using a universal electromechanical tensile tester (ST-DATEC, China) and a digital source meter (Keithley 2450, US). During the test, the hydrogel strain sensor was connected to a circuit, and the real-time resistances of the hydrogel sensor were recorded by the digital source meter during the stretching and the relax process of the hydrogel. The relative resistance change of the hydrogel was calculated by the following equation (10):

$$\frac{\Delta R}{R_0} = \frac{R - R_0}{R_0} \times 100\% \tag{10}$$

where R is the dynamic resistance of the hydrogel and R_0 is the original resistance of the hydrogel without strain. In addition, the sensitivity of the hydrogel sensor is evaluated by the gauge factor (GF) as follows (11):

$$GF = \frac{\Delta R}{R_0} \times \frac{1}{\varepsilon} \tag{11}$$

where ε is the corresponding elongation of the hydrogel.

The resistance changes of the cylindrical hydrogel sensors (8 mm in height and 10 mm in diameter) under compressive strain were evaluated as well, and the sensitivity S was defined by the slope of the resistance change curves. All the measurements were carried out at 25 °C.

For human motions detection, the assembled hydrogel sensors were attached to different joints of human body such as fingers, throat, wrist, elbow and knee. The real-time resistance changes caused by movement of the joint were recorded by the digital source meter. The experiment was completed by assistance of the informed volunteers.

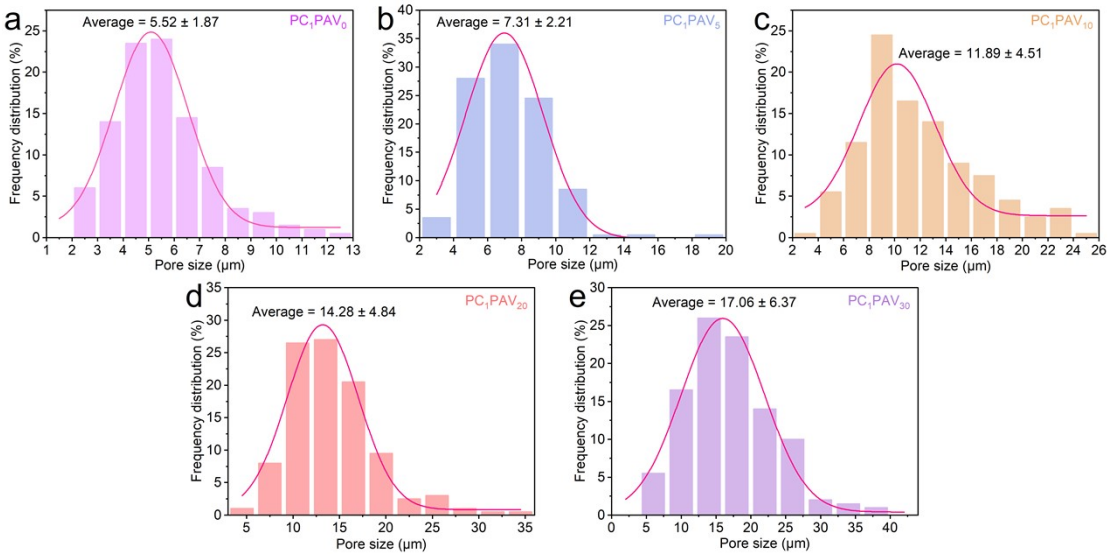

Fig. S1. Pore size distribution of PCPAV hydrogels.

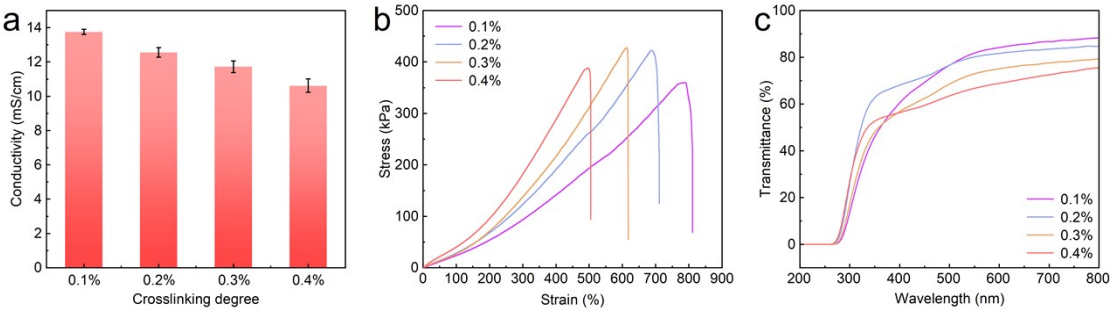

Fig. S2. (a) The conductivity, (b) stress-strain curves during tensile tests and (c) transparency of hydrogels that prepared with different crosslinking degrees.

The effect of the crosslinking degree of AAm and VBIMBr to the electrical conductivity, mechanical properties and light transmission was first investigated. The testing results of conductivity, tensile properties and light transmission of the PCPAV hydrogels with 0.1%-0.4% degree of cross-linking were shown in Fig. S2a, b and c, respectively. It can be seen that ionic conductive hydrogels with a higher degree of crosslinking exhibited lower electrical conductivity, lower tensile strength, and lower

light transmission, which were primarily due to their denser and stiffer polymer crosslinking network.[1]

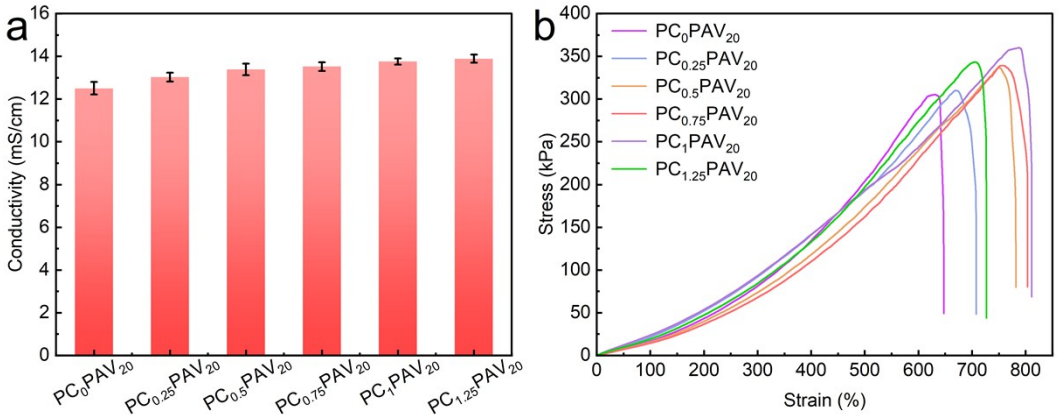

Fig. S3. (a) The conductivity, (b) stress-strain curves during tensile tests of hydrogels that prepared with different content of CMC.

In addition, the effects of CMC addition on the electrical conductivity and mechanical properties of the hydrogels were investigated. As shown in Fig. S3a, the electrical conductivity of the hydrogels increased with increasing addition of CMC, which provides freely movable Na^+ ions to the hydrogels, and the carboxyl groups on the CMC chains could attract counter ions, creating more hopping sites for ion migration.[2] Fig. S3b illustrated the mechanical properties of the hydrogels. The tensile strength of the hydrogels firstly increased and then decreased with increasing content of CMC. The maximum tensile strength as well as largest elongation at break were observed with 1% the CMC addition. This might be due to the fact that the addition of CMC increased the intermolecular and intramolecular hydrogen bonds and electrostatic

interactions between the polymer chains, which improved the mechanical properties of the hydrogels.

Therefore, by overall consideration of the conductivity, mechanical and light transmission properties of the hydrogel, the crosslinking degree of PCPAV hydrogels was chosen to be 0.1% and the CMC addition was set to be 1%.

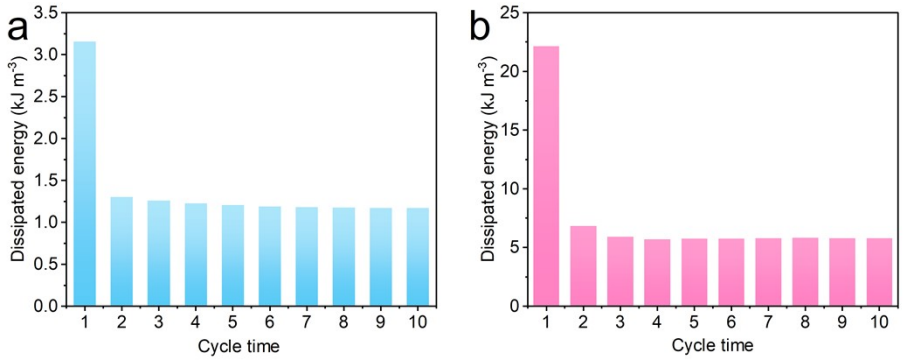

Fig. S4. (a) Dissipated energy of the PC_1PAV_{20} hydrogel at 100% strain for 10 consecutive loaded-unloaded tensile cycles; (b) Dissipated energy of PC_1PAV_{20} hydrogel at 50% strain for 10 consecutive loaded-unloaded compression cycles.

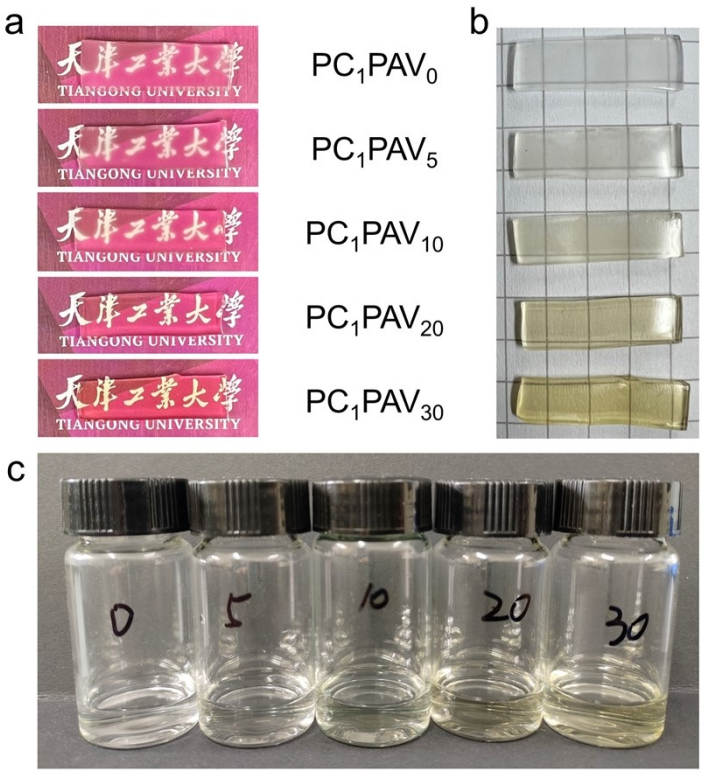

Fig. S5. (a) and (b) The photographs of the macroscopic appearance of PCPAV hydrogels. (c) The mixed VBIMBr/H_2O solutions with different VBIMBr contents.

Figs. S5a and b showed the macroscopic appearance of PCPAV hydrogels. It could be clearly seen that the transparency of the PC_1PAV_0 hydrogel was significantly different from that of other four PCPAV hydrogels with different VBIMBr additions from the comparison of the photos. After being covered by the hydrogel, a clearer pattern detail could be observed in the hydrogel with higher VBIMBr additions (Fig. S5a). It is noteworthy that the content of VBIMBr maintains a relatively high transparency despite its effect on the color of the hydrogels (Fig. S5b). It should be noted that, the yellow color of the hydrogel with high VBIMBr concentration is due to the yellow color of the VBIMBr solution. After VBIMBr dissolved in water, the VBIMBr solution was in yellow color (Fig. S5c).

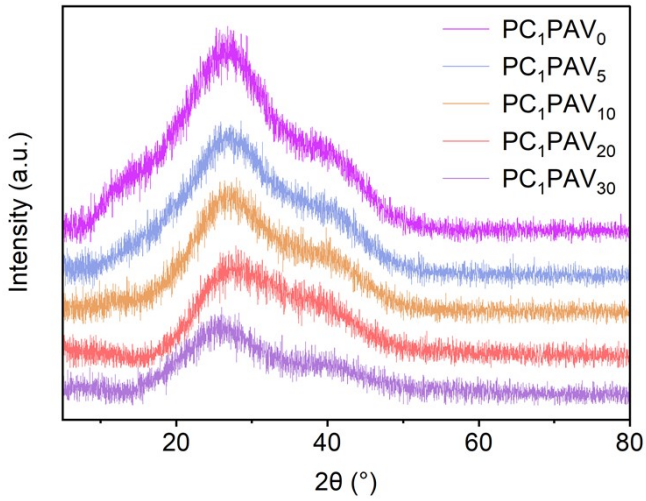

Fig. S6. XRD diffractograms of PCPAV hydrogels.

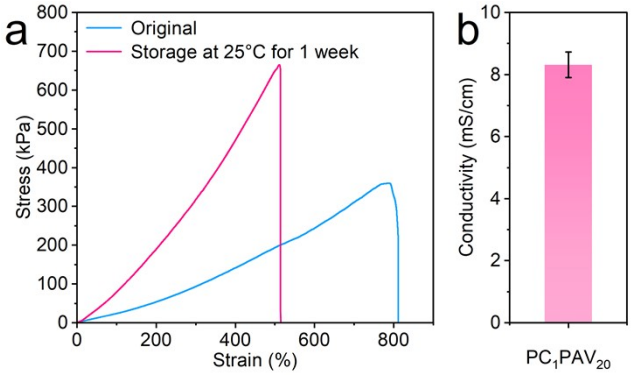

Fig. S7. The mechanical properties (a) and electrical conductivity (b) of PC_1PAV_{20} hydrogel after one week storage at 25 °C.

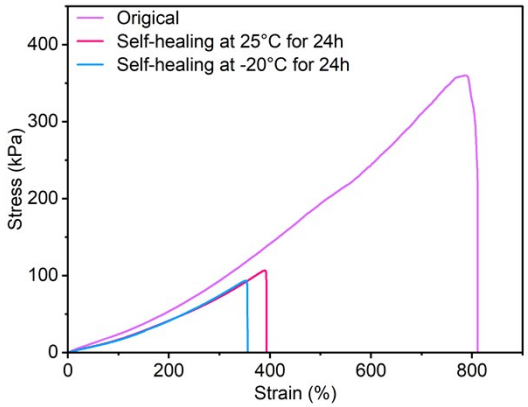

Fig. S8. Mechanical properties of PC_1PAV_{20} hydrogel after 24 h of self-healing at 25 °C and -20 °C.

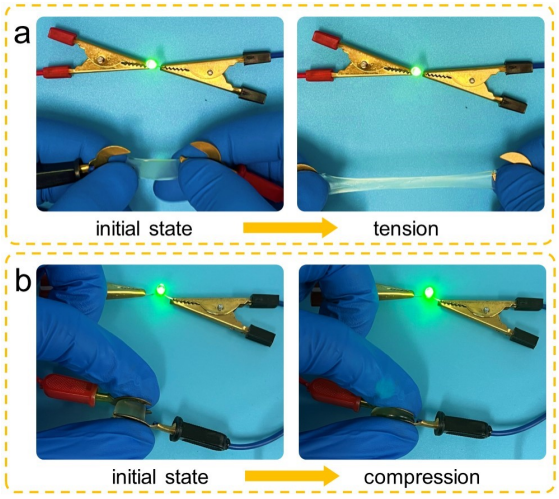

Fig. S9. Using PC_1PAV_{20} hydrogel as a conductor, the brightness of LED varied with (a) tensile and (b) compressive.

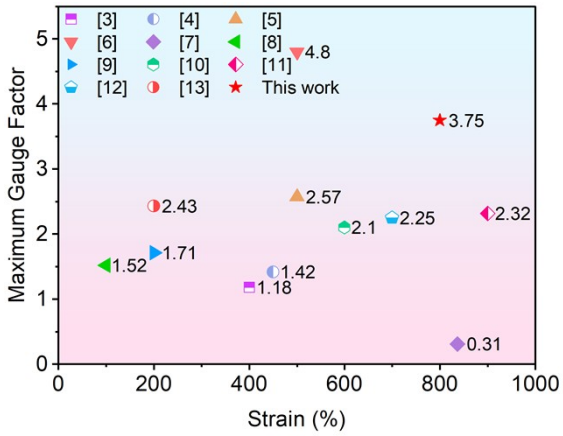

Fig. S10. Comparison of GF of PCPAV hydrogels with published literature.[3-13]

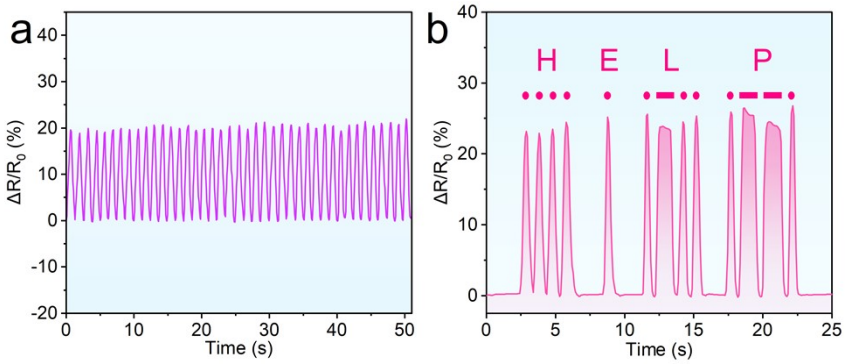

Fig. S11. The sensing properties of PC_1PAV_{20} hydrogel after one week storage at 25 °C.

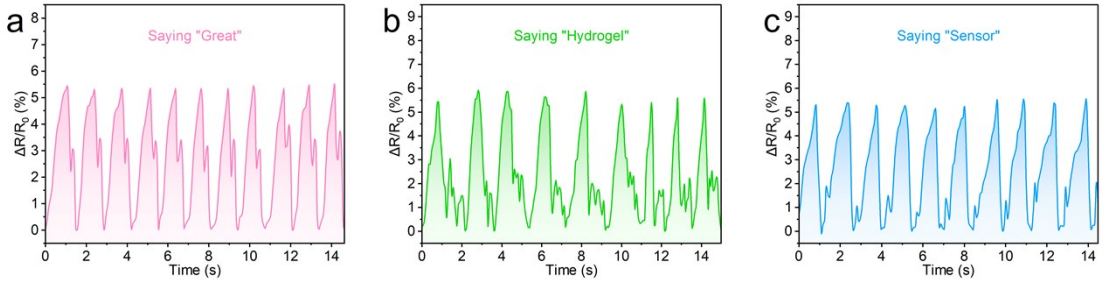

Fig. S12. Pronouncing “Great” (a), “Hydrogel” (b), and “Sensor” (c).

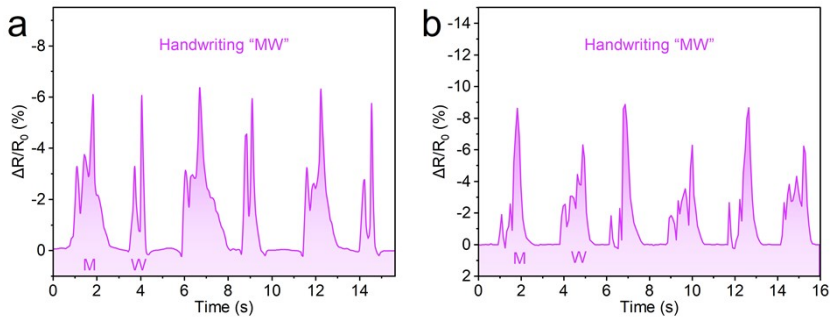

Fig. S13. The relative resistance changes when two volunteers wrote the same letter combination "MW".

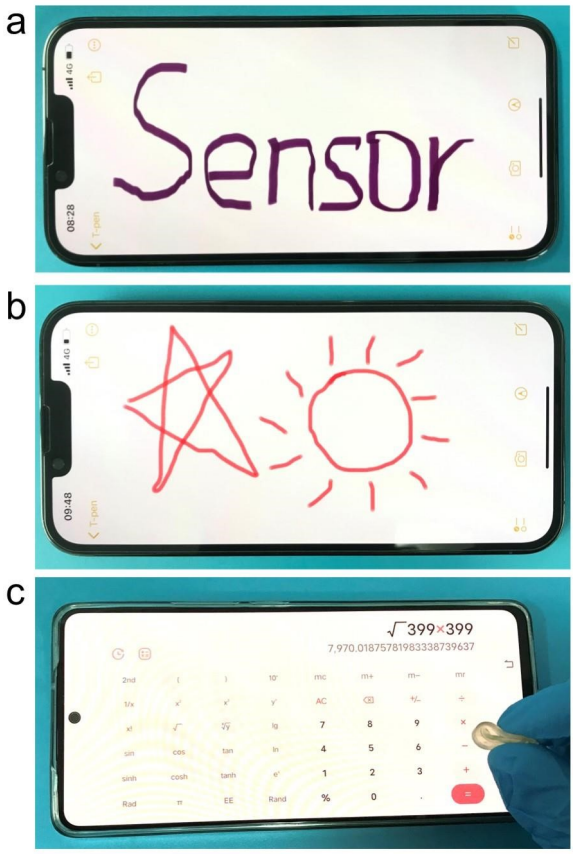

Fig. S14. The PC_1PAV_{20} hydrogel was used as a T-pen to write "Sensor" on smartphone screens (a), draw pentagrams and suns (b), and tap the screen to perform calculations (c).

Table S1. Crystallinity of PCPAV hydrogels

Sample	Crystallinity (%)
PC_1PAV_0	14.34
PC_1PAV_5	12.81
PC_1PAV_{10}	10.40
PC_1PAV_{20}	6.40
PC_1PAV_{30}	3.62

Table S2. Comparison of the conductivity of existing ionic conductive hydrogels

Hydrogel	Conductive component	Conductivity (mS/cm)	Refs
P(NIPAm-*co*-AAm)/PEI/SDS/NaCl	Na^+, Cl^-	2.2	14
PNA/PVP/TA/Fe^{3+}	Fe^{3+}	7.9	15
PVA/PMAA/Fe^{3+}	Fe^{3+}	10.1	16
P(AA_5-$APA_{0.14}$)-Fe^{3+}6.1	Fe^{3+}	5.5	2
PAA-*r*-BVIT/PEO	1-butyl-3-vinylimidazole (BVIT)	0.36	17
SA/LM/PAM/SDS/NaCl	Na^+, Cl^-	8.0	18
PVA/SS/Na_3Cit	Na^+, Cit^{3-}	8.3	19
PVA-PAANa-PAH	Na^+, Cl^-	3.0	20
P(AM-BA-A-ACG)/LiCl/SDS	Na^+, Li^+, Cl^-	13.5	21
PVA-CS-PA	phytic acid (PA, free hydrogen ions (H^+))	5.1	22
PU/P(SBMA-*co*-AM)/KCl	carboxylate ions, $^+NHEt_3$, K^+, Cl^-	1.2	23
Ca-XG/P(AA-*co*-OMA)	Ca^{2+}, Na^+, Cl^-	5.0	24
PVA/CNF/TA/Gly/NaCl	Na^+, Cl^-	8.6	25
PAAm/PAA-Fe^{3+}/NaCl	Fe^{3+}, Na^+, Cl^-	7.2	26
CS-P(AM-*co*-AA)/$FeCl_3$	Fe^{3+}, Cl^-	3.1	27
PCPAV	VBIMBr (imidazole cations, Br^-)， Na^+	15.2	This work

Table S3. Comparison of freezing points of existing anti-freezing conductive hydrogels

Hydrogel	Antifreeze	Freezing point (°C)	Refs
PAM/SA/LiCl	LiCl	-40.9	28
PAHS	LiCl	-25.2	29
PVA/EG	EG	-20	30
SPAE	[Emim]Ac, $AlCl_3$	-12.1	31
P(AAS-DAAM)/PVA	NaCl	-32.3	32
AA@CS-Al/Gly	Al^{3+}, Gly	-39.8	33
HPMC-*g*-P(AM/AA/C_{18})–$ZnCl_2$	$ZnCl_2$	-32	34
CS/P(AA-*co*-SS)/NaCl	NaCl	-33.3	35
PHEAA/SF-LiCl	LiCl	-30	36
PVA–EG50%	EG	-32.12	37
PCPAV	VBIMBr	-45.5	This work

Table S4. The feed ratio of PCPAV ionic conductive hydrogels

Sample	PVA solution (8wt%, mL)	CMC (g)	AAm (g)	VBIMBr (g)	MBAA (g)	APS (g)
PC_1PAV_0 [a]	10	0.1	2.0	0	0.002	0.02
PC_1PAV_5 [a]	10	0.1	2.0	0.5	0.0025	0.025
PC_1PAV_{10} [a]	10	0.1	2.0	1.0	0.003	0.03
PC_1PAV_{20} [a]	10	0.1	2.0	2.0	0.004	0.04
PC_1PAV_{30} [a]	10	0.1	2.0	3.0	0.005	0.05
PC_1PAV_{20}-0.2 [b]	10	0.1	2.0	2.0	0.008	0.04
PC_1PAV_{20}-0.3 [b]	10	0.1	2.0	2.0	0.012	0.04
PC_1PAV_{20}-0.4 [b]	10	0.1	2.0	2.0	0.016	0.04
PC_0PAV_{20} [a]	10	0	2.0	2.0	0.004	0.04
$PC_{0.25}PAV_{20}$ [a]	10	0.025	2.0	2.0	0.004	0.04
$PC_{0.5}PAV_{20}$ [a]	10	0.05	2.0	2.0	0.004	0.04
$PC_{0.75}PAV_{20}$ [a]	10	0.075	2.0	2.0	0.004	0.04
$PC_{1.25}PAV_{20}$ [a]	10	0.125	2.0	2.0	0.004	0.04

Note: [a] represents the hydrogel sample with 0.1% crosslinking, and [b] represents the hydrogel sample with high crosslinking, where the number that follows represents the crosslinking density, e.g., PC_1PAV_{20}-0.2 represents the hydrogel sample with 0.2% crosslinking.

References

1 X. Sui, H. Guo, P. Chen, Y. Zhu, C. Wen, Y. Gao, J. Yang, X. Zhang and L. Zhang, *Adv. Funct. Mater.*, 2020, **30**, 1907986.

2 K. Shen, K. Xu, M. Zhang, J. Yu, Y. Yang, X. Zhao, Q. Zhang, Y. Wu, Y. Zhang and Y. Cheng, *Chem. Eng. J.*, 2023, **451**, 138525.

3 Y. Peng, M. Pi, X. Zhang, B. Yan, Y. Li, L. Shi and R. Ran, *Polymer*, 2020, **196**, 122469.

4 J. Bai, R. Wang, X. Wang, S. Liu, X. Wang, J. Ma, Z. Qin and T. Jiao, *Cell Rep. Phys. Sci.*, 2021, **2**, 100623.

5 C. Zhao, L. Liu, M. Guo, Z. Sun, Y. Chen, Y. Wu, Y. Li, D. Xiang, H. Li and Z. Li, *Colloids. Surf. A: Physicochem. Eng. Asp.*, 2022, **652**, 129803.

6 Z. Bei, Y. Chen, S. Li, Z. Zhu, J. Xiong, R. He, C. Zhu, Y. Cao and Z. Qian, *Chem. Eng. J.*, 2023, **451**, 138675.

7 Z. Bian, Y. Li, H. Sun, M. Shi, Y. Zheng, H. Liu, C. Liu and C. Shen, *Carbohyd. Polym.*, 2023, **301**, 120300.

8 Z. Nie, K. Peng, L. Lin, J. Yang, Z. Cheng, Q. Gan, Y. Chen and C. Feng, *Chem. Eng. J.*, 2023, **454**, 139843.

9 C. Qian, Y. Li, C. Chen, L. Han, Q. Han, L. Liu and Z. Lu, *Chem. Eng. J.*, 2023, **454**, 140263.

10 H. Chen, J. Huang, J. Liu, J. Gu, J. Zhu, B. Huang, J. Bai, J. Guo, X. Yang and L. Guan, *J. Mater. Chem. A*, 2021, **9**, 23243-23255.

11 M. Wu, J. Chen, Y. Ma, B. Yan, M. Pan, Q. Peng, W. Wang, L. Han, J. Liu and H. Zeng, *J. Mater. Chem. A*, 2020, **8**, 24718-24733.

12 Y. Gao, Y. Gao, Z. Zhang, Y. Wang, X. Ren, F. Jia and G. Gao, *J. Mater. Chem. C*, 2022, **10**, 12873-12882.

13 X. Yu, H. Zhang, Y. Wang, X. Fan, Z. Li, X. Zhang and T. Liu, *Adv. Funct. Mater.*, 2022, **32**, 2204366.

14 L. Bai, Y. Jin, X. Shang, H. Jin, W. Zeng and L. Shi, *Chem. Eng. J.*, 2023, **456**, 141082.

15 Q. Pang, H. Hu, H. Zhang, B. Qiao and L. Ma, *ACS Appl. Mater. Interfaces*, 2022, **14**, 26536-26547.

16 X. Li, J. Wang, Y. Lin, Y. Cheng, W. Han, G. Yuan and H. Jia, *Colloids. Surf. A: Physicochem. Eng. Asp.*, 2022, **635**, 128091.

17 A. Wang, Y. Wang, B. Zhang, K. Wan, J. Zhu, J. Xu, C. Zhang and T. Liu, *Chem. Eng. J.*, 2021, **411**, 128506.

18 S. Yazdani, M. Khan, A. Shahzad, L. A. Shah and D. Ye, *Sensor. Actuat. A: Phys.*, 2023, **350**, 114148.

19 F. Wang, Z. Li, J. Guo, L. Liu, H. Fu, J. Yao, I. Krucińska and Z. Draczyński, *ACS Appl. Polym. Mater.*, 2022, **4**, 618-626.

20 W. J. Yang, R. Zhang, X. Guo, R. Ma, Z. Liu, T. Wang and L. Wang, *J. Mater. Chem. A*, 2022, **10**, 23649-23665.

21 X. Di, J. Li, M. Yang, Q. Zhao, G. Wu and P. Sun, *J. Mater. Chem. A*, 2021, **9**, 20703-20713.
22 C. Liu, R. Zhang, Y. Wang, J. Qu, J. Huang, M. Mo, N. Qing and L. Tang, *J. Mater. Chem. A*, 2023, **11**, 2002-2013.
23 X. Li, E. Zhang, J. Shi, X. Xiong, J. Lin, Q. Zhang, X. Cui, L. Tan and K. Wu, *Macromol. Rapid Comm.*, 2021, **42**, 2100457.
24 H. Song, B. Zhang, Q. Feng, D. H. Nguyen, C. Zhang and T. Liu, *J. Polym. Sci.*, 2022, **60**, 2817-2827.
25 M. Li, Y. Yang, C. Yue, Y. Song, M. Manzo, Z. Huang and L. Cai, *Cellulose*, 2022, **29**, 1897-1909.
26 S. Li, H. Pan, Y. Wang and J. Sun, *J. Mater. Chem. A*, 2020, **8**, 3667-3675.
27 H. Liu, X. Wang, Y. Cao, Y. Yang, Y. Yang, Y. Gao, Z. Ma, J. Wang, W. Wang and D. Wu, *ACS Appl. Mater. Interfaces*, 2020, **12**, 25334-25344.
28 C. Zhang, J. Wang, S. Li, X. Zou, H. Yin, Y. Huang, F. Dong, P. Li and Y. Song, *Eur. Polym. J.*, 2023, **186**, 111827.
29 Y. Zhang, H. Liu, P. Wang, Y. Yu, M. Zhou, B. Xu, L. Cui and Q. Wang, *Eur. Polym. J.*, 2023, **186**, 111824.
30 Z. Li, F. Yin, W. He, T. Hang, Z. Li, J. Zheng, X. Li, S. Jiang and Y. Chen, *Int. J. Biol. Macromol.*, 2023, **230**, 123117.
31 L. Lu, Z. Huang, X. Li, X. Li, B. Cui, C. Yuan, L. Guo, P. Liu and Q. Dai, *Int. J. Biol. Macromol.*, 2022, **213**, 791-803.
32 R. Liu, J. Chen, Z. Luo, X. Zhang, W. Chen and Z. Niu, *React. Funct. Polym.*, 2022, **172**, 105197.
33 L.-Y. Zeng, X.-C. Wang, Y. Wen, H.-M. Chen, H.-L. Ni, W.-H. Yu, Y.-F. Bai, K.-Q. Zhao and P. Hu, *Carbohyd. Polym.*, 2023, **300**, 120229.
34 X. Zhao, H. Wang, J. Luo, G. Ren, J. Wang, Y. Chen and P. Jia, *ACS Appl. Polym. Mater.*, 2022, **4**, 1784-1793.
35 S. Chen, J. Huang, Z. Zhou, Q. Chen, M. Hong, S. Yang and F. Heqing, *Ind. Eng. Chem. Res.*, 2021, **60**, 6162-6172.
36 X. Sun, S. He, M. Yao, X. Wu, H. Zhang, F. Yao and J. Li, *J. Mater. Chem. C*, 2021, **9**, 1880-1887.
37 C. Niu, H. Zhang, B. Yang and H. Sun, *New J. Chem.*, 2021, **45**, 14392-14400.